# New Trithia- and Dithioxa-macrocycles with Biphenyl Fused into the Backbone: Structures, and Molecular Modelling Studies

**Joyce C. Lockhart,*[a] David P. Mousley,[a] George A. Forsyth,[a] Francesc Teixidor,[b] Maria P. Almajano,[b] Luis Escriche,[b] Jaume Casabo,[b] Reijo Sillanpää[c] and Raikko Kivekäs[d]**

[a] *Department of Chemistry, Bedson Building, The University, Newcastle upon Tyne, UK NE1 7RU*
[b] *Department de Quimica Universitat Autònoma de Barcelona and Institut de Ciencia dels Materials de Barcelona, 08193 Bellaterra, Spain*
[c] *Department of Chemistry, University of Turku, FIN-20500, Turku, Finland*
[d] *Inorganic Chemistry Laboratory, Department of Chemistry, FIN-00017, University of Helsinki, Helsinki, Finland*

Two novel thiamacrocycles have been synthesised with a biphenyl unit and SCCSCCS or SCCOCCS linkers in the ring backbone. Their crystal structures have been determined, showing the trithia ligand to have both SCCS torsions *anti* (*a*) whilst the dithioxa ligand has both its SCCO torsions in a plus *gauche* ($g^+$) conformation. Molecular dynamics simulations of these two ligands at several temperatures again show differences, the trithia being more rigid; in addition, the conformations predominating in the dynamics simulations of the dithioxa ligand are different from that of the crystal structure. No conformation occurred with any frequency which could be considered to have potential as a tridentate ligand (all-*endo* sulfurs or oxygens). Derivatives built with additional *o*-Me substituents were also examined. The cavity size provided by two of the ligands (operating as tridentate ligands) was calculated, and the implications for coordination of the new ligands are considered.

The dynamic structure of biphenyl **1** has intrigued generations of chemists: the more recent applications of biphenyl and derivatives in liquid crystals have ensured continuance of this study. A wealth of information has been obtained relating to the structure of the parent and many substituted biphenyls, in particular the twist angle between the two phenyl planes, from X-ray diffraction of crystals, electron diffraction of gases, and liquid crystal NMR determinations, and also from solution NMR relating to the activation energies for racemisation, which may be correlated with the steric hindrance of the substituents present. It has been apparent for over 30 years that particular intermolecular forces in the crystal may cause the solid state structure (first definitively determined to be planar, with the inter-ring torsion 0° by Trotter)[1] to differ from that where the biphenyl is free to twist round its connecting C–C link, as in the gas phase electron diffraction results first determined by Bastiansen,[2] subsequently confirmed with improved methods.[3] NMR data in a nematic phase have been interpreted in terms of torsions of 34 or 37.2° depending on the mode of calculation,[4] and there have been several theoretical studies;[5] a recent paper[6] summarises the current situation for biphenyl. Field, Skelton, Sternhell and White[7] have also shown that for substituted biphenyls, their own results from NMR studies in nematic liquid crystals were consistently different from those from their X-ray data. In the molecules described in this paper, the chiral biphenyl unit is incorporated, thus the angle of twist of the two phenyl rings is a source of regulation of the stereochemistry of the thiacrown moiety. Earlier examples[8,9] used binaphthyl or biphenyl units in crown ether chemistry.

Thioether polydentate and macrocyclic ligands are of great interest in coordination chemistry generally, owing to their ability to coordinate to soft metal ions.[10,11] Some of the ligands studied by our groups have recently attracted much attention for $Ag^+$ detection.[12] In this area of research, we have developed ion selective electrodes (ISE) for the silver ion mainly based on bisthiamethylene benzene derivatives **2** (cyclophanes). Similar molecules have been found elsewhere[13] to be effective extractants for soft metal ions $Ag^+$ and $Cu^{2+}$, the *meta* derivatives having especial properties with regard to $Ag^+$. The cyclophanes **2** have proved to be extremely efficient for $Ag^+$ monitoring, and have provided $K^{pot}_{Ag,M}$ of the order of $10^{-6}$. This high selectivity, coupled with fast response times (< 2 s) and reproducibility (over a lifetime of more than three years) provides very reliable ISEs for $Ag^+$. No great differences have been found between these cyclophanes **2**, where X = S, O and $CH_2$.

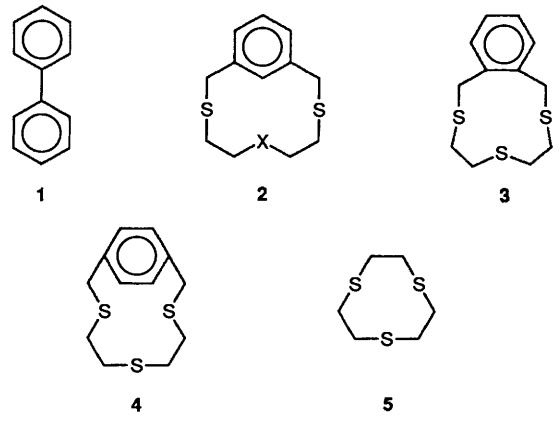


**1** **2** **3** **4** **5**

The conformational possibilities provided by the *meta*-substituted molecule **2** (X = S, *m*-S3) and in the *ortho* and *para* analogues **3**, and **4** have been recently studied in our laboratories.[14] In addition, the coordinating similarity between the trithianonane ligand, **5** (9S3) and **3** (*o*-S3) has been demonstrated.[15] This similarity led us to study **5** (9S3) as an ionophore in ISEs for $Cu^{2+}$ detection.[16] The results obtained with **5** are very encouraging, with Nernstian responses and low detection limits ($a = 10^{-6}$), in spite of the short lifetime of the

ISE as a result of leakage of **5** from the membrane. We have also recently examined the relation between the hole size, calculated by molecular mechanics methods following the work of Drew and co-workers,[17] of several thiamacrocycles related to **2** (X = S), noting that this ligand should be suitable for the largest of the soft metal ions,[18] unlike **5** (9S3), which has been shown[19] to be suitable for the smaller first row d-block ions like Cu. With the aim of preparing new thiamacrocycles, related to the 9S3 and *m*-S3 series, which might be capable of tridentate facial or meridional coordination to soft metal ions, and which might contribute to the better understanding of the phenomena of ion recognition, we have produced the strained molecules 11-oxa-8,14-dithiatricyclo[19,0,$0^{1,6}$,$0^{16,21}$] heneicosa-1(2),3,5,16(17),-18,20-hexene (BIFS2O) **6** and 8,11,14-trithiatricyclo[19,0,-$0^{1,6}$,$0^{16,21}$] heneicosa-1(2),3,5,16(17),18,20-hexene (BIFS3) **7**, and studied their structures by crystallography. Molecular dynamics (MD) simulations were performed on **6** and **7** and the screen-built derivatives with the respective remaining *ortho* positions of the biphenyl blocked by Me groups, **8** and **9**. Opportunity arises here to compare the X-ray crystal studies with molecular modelling results (which represent a gas-phase structure), and, using MD, to visualise the limited movement of the phenyl–phenyl torsion on the ps to ns timescale. This is of interest in relation to the much longer timescales required for racemisation, *i.e.* the change of sign of this torsion, proceeding through a putative transition state value of 0°.

## Experimental

*General.*—Microanalyses (C, H, S) were performed on a Perkin-Elmer 240-B instrument. Proton NMR spectra were run on Bruker AM400 and WM300WB instruments in $CDCl_3$ solution. Unless specifically mentioned, the syntheses were performed under a nitrogen atmosphere, using dehydrated and deoxygenated solvents. Solvents were placed under vacuum to eliminate the dissolved oxygen. 2,2′-Bis(bromomethyl)-1,1′-biphenyl, bis(2-mercaptoethyl) ether and bis(2-mercaptoethyl) sulfide are commercially available.

*Synthesis of Cyclophanes* 11-*Oxa*-8,14-*dithiatricyclo*-[19,0,0,$^{1,6}$,$0^{16,21}$]*heneicosa*-1(2),3,5,16(17),18,20-*hexene* (*BIFS2O*) **6** *and* 8,11,14-*Trithiatricyclo*[19,0,$0^{1,6}$,$0^{16,21}$]-*heneicosa*-1(2),3,5,16(17),18,20-*hexene* (*BIFS3*) **7**.—Under a nitrogen atmosphere and high dilution conditions, a solution (A) of KOH (29.4 mmol) and bis(2-mercaptoethyl) ether (14.7 mmol) (for synthesis of **6**) or bis(2-mercaptoethyl) sulfide (14.7 mmol) (for synthesis of **7**) in butan-1-ol (50 $cm^3$) was mixed in boiling butan-1-ol (1500 $cm^3$) with a second solution (B) of 2,2′-bis(bromomethyl)-1,1′-biphenyl (14.7 mmol) at a rate of 3 $cm^3$ $h^{-1}$. The KBr formed was filtered off and the resulting solution was evaporated to dryness. The resulting oily material was taken up in dichloromethane (50 $cm^3$), washed with saturated aq. $Na_2CO_3$, then water and dried ($Na_2SO_4$, 8 h) and the solvent removed under reduced pressure. The dry residue was dissolved in toluene (5 $cm^3$) and chromatographed (silica gel). The fraction eluted with toluene was separated and taken to dryness to obtain a yellow oil which was dissolved in cold dichloromethane (5 $cm^3$) and allowed to stand at −5 °C. After 48 h a first crop of white crystalline solid appeared, which was filtered off and vacuum dried. Crystals were in both cases suitable for X-ray diffraction analysis. Yield: 0.33 g (7%) BIFS2O **6**; 0.65 g (13%) BIFS3 **7** [Found: C, 67.9; H, 5.9; S, 19.7. $C_{18}H_{20}OS_2$ (BIFS2O **6**) requires C, 68.4; H, 6.4; S, 20.2%. Found: C, 64.9; H, 5.8; S, 29.3. $C_{18}H_{20}S_3$ (BIFS3 **7**) requires C, 65.1; H, 6.1; S, 28.9%]. $\delta_H$(300 and 400 MHz; $CDCl_3$) BIFS2O **6**, 2.65 (4, t, $-OCH_2CH_2S-$), 2.39 (4, t, $-OCH_2CH_2S-$), 3.47 (4, dd, $-SCH_2Ar$), 7.12–7.91 (8, m, Ar); BIFS3 **7**, 2.35–2.55 (8, ABCD pattern, $-SCH_2CH_2S-$), 3.66 (4, AB pattern $J$ −15.84 Hz, $-SCH_2Ar$), 7.10 (2, d, Ar), 7.28 (2, t, Ar), 7.42 (2, t, Ar), 7.96 (2, d, Ar); $\delta_C$(75 and 100 MHz; $CDCl_3$) BIFS2O **6**, 27.6 ($-OCH_2CH_2S-$), 33.7 ($-SCH_2Ar$), 72.8 ($-OCH_2CH_2S-$), 126.2, 127.7, 128.4, 131.0, 135.6, 140.5 (Ar); BIFS3 **7**, 30.1, 30.2 ($-SCH_2CH_2S-$), 32.3 ($-SCH_2Ar$), 126.3, 128.1, 129.3, 130.7, 134.9, 139.8 (Ar).

*Isolation of the mono-sulfide side-product* **10**. To the remaining filtrate solution was added diethyl ether (2 $cm^3$). After 8 h at −5 °C a second crop of white microcrystalline solid appeared, which was filtered off and vacuum dried. The products obtained are, in both of the above syntheses, the monosulfide, BIFS, **10**. Yield: 1.09 g (35%) in BIFS2O synthesis and 0.87 g (28%) in BIFS3 synthesis [Found: C, 78.9; H, 5.5; S, 16.3. $C_{14}H_{12}S$ (BIFS) requires C, 79.2; H, 5.7; S, 15.8%]. $\delta_H$(400 MHz; $CDCl_3$) 3.41 (4, dd, $-S-CH_2-Ar$), 7.24–7.40 (8, m, Ar); $\delta_C$(100 MHz; $CDCl_3$) 31.3 ($-S-CH_2-Ar$), 127.7, 128.3, 128.4, 135.6, 140.6 (Ar).

*Crystal Determination for* **6**.—Single crystal data collection was performed at 295 K with Nicolet P3F diffractometer using monochromatised Mo-Kα radiation ($\lambda$ = 0.710 69 Å). A prismatic colourless crystal with dimensions 0.50 × 0.40 × 0.28 mm was used. The compound $C_{18}H_{20}OS_2$, $M_r$ = 316.5, crystallises in the triclinic system, space group $P\bar{1}$(no. 2), $a$ = 7.505(1), $b$ = 8.464(1), $c$ = 13.743(2) Å, $\alpha$ = 88.03(1), $\beta$ = 87.40(1), $\gamma$ = 72.87(1)°, $U$ = 833.2(2) $Å^3$, $Z$ = 2, $D_c$ = 1.261 g $cm^{-3}$, $F(000)$ = 336, $\mu$(Mo-Kα) = 3.0 $cm^{-1}$.

The unit cell parameters were determined by least-squares refinements of 25 carefully centred reflections ($16 < 2\theta < 26°$). The data obtained were corrected for Lorentz and polarisation effects and for dispersion. 3448 Unique reflections were collected by $\omega$ scan mode ($2\theta_{max}$ = 53°). Of those 2961 were considered as observed according to the criteria $|F| > 3\sigma(F)$. The three check reflections monitored after every 60 reflections showed only statistical fluctuations during the course of the data collection.

The structure was solved by direct methods by using the SHELXS86 program.[20] Least-squares refinements and all subsequent calculations were performed using the XTAL program system,[21] which minimised the function $\Sigma w(\Delta F)^2$ where [$w = 1/\sigma^2(F_o)$]. Refinement of all atoms, with anisotropic temperature factors for the non-hydrogen atoms and isotropic temperature factors for the hydrogen atoms reduced the $R$ value to 0.046 ($R_w$ = 0.045) for 270 parameters. Neutral atomic scattering factors were those included in the program. Fractional atomic coordinates for **6** have been deposited.*

*Crystal Determination for* **7**.—Single crystal data collection was performed at 296(1) K using a Rigaku AFC5S diffractometer, monochromatised Mo-Kα radiation ($\lambda$ = 0.710 69 Å). A colourless bar-like crystal with dimensions 0.12 × 0.18 × 0.34 mm was used. The compound $C_{18}H_{20}S_3$, $M_r$ = 332.554, crystallises in the triclinic space group $P\bar{1}$(no. 2), $a$ = 10.126(1), $b$ = 10.175(2), $c$ = 9.543(1) Å, $\alpha$ = 108.56(1), $\beta$ = 95.82(1), $\gamma$ = 65.54(1)°, $U$ = 847.9(3) $Å^3$, $Z$ = 2, $D_c$ = 1.302 g $cm^{-3}$, $F(000)$ = 352, $\mu$(Mo-Kα) = 4.11 $cm^{-1}$.

The unit cell parameters were determined by least-squares refinements of 25 carefully centred reflections ($39 < 2\theta < 47°$). The data obtained were corrected for Lorentz and polarisation effects and for dispersion. A total of 3157 reflections were collected by $\omega$–$2\theta$ scan mode ($2\theta_{max}$ = 50°), giving 2973 unique reflections ($R_{int}$ = 0.011). Of those 2330 were considered as observed according to the criteria

* For details of the deposition scheme see 'Instructions for Authors (1994)', *J. Chem. Soc., Perkin Trans. 2*, issue 1, 1994.

**Table 1** Energies of minimised starting structures

| CHARMm energy/ kcal mol$^{-1}$ [a] | 6 | 7 | 8 | 9 |
|---|---|---|---|---|
| Bond energy | 3.21 | 3.38 | 3.78 | 3.91 |
| Angle energy | 2.26 | 1.56 | 2.38 | 1.84 |
| Dihedral energy | 7.94 | 6.07 | 8.19 | 7.86 |
| Improper energy | 0.20 | 0.02 | 0.14 | 0.06 |
| Lennard Jones energy | 17.45 | 17.88 | 17.84 | 17.79 |
| Electrostatic energy | −6.85 | −10.60 | −10.85 | −14.28 |
| Total energy | 24.12 | 18.30 | 21.46 | 17.17 |

[a] 1 kcal = 4.184 kJ.

$I > 2\sigma(I)$. The three check reflections monitored after every 100 reflections showed only statistical fluctuations during the course of the data collection.

The structure was solved by direct methods using MITRIL.[22] Least-squares refinements and all subsequent calculations were performed using the TEXSAN crystallographic software package,[23] which minimised the function $\Sigma w(\Delta F)^2$ where $w = 1/\sigma^2(F_o)$. Refinement of all non-hydrogen atoms with anisotropic and hydrogen atoms with fixed isotropic temperature parameters (1.2 times $B_{eq}$ of carrying atom) reduced the $R$ value to 0.033 ($R_w$ = 0.040 for 250 parameters). Neutral atomic scattering factors were those included in the program. The structure was plotted with ORTEP.[24] Fractional atomic coordinates for **7** have been deposited.*

*Molecular Dynamics.*—Each of the four structures **6**, **7**, **8** and **9** was simulated at 300, 350 and 470 K for 610 ps. For **6** and **7** atomic coordinates from the structures were used as input for the simulations; for **8** and **9** coordinates were obtained by replacement of the relevant two hydrogen atoms of **6** and **7** with methyl groups using the Molecular Editor of QUANTA. The protocol described by Lockhart and Tomkinson[25] was used, with version 21.3 of CHARMm and QUANTA,[26] supplied by Polygen and running on an SG IRIS 4D20G. No changes were made to the CHARMm force field. The molecules were assigned CHARMm atom types as shown in the Supplementary Data, and all four structures were minimised as shown in Table 1. Simulations at 470 K (following ref. 14) were first performed and indicated very rapid movement with additional conformations differing from that of the starting crystal conformation accessible within 600 ps simulation both for **6** and for **7**. Simulations at 300, 350 and 470 K for the structures **6**, **7**, **8** and **9** are reported.

*Calculation of Optimal M–S Distances.*—Minimisations were performed by the method of Drew, Hollis and Yates,[17] varying the M–S bond length from 2 to 3.4 Å, in steps of 0.1 Å. A very large M–S bond-stretching force constant was used, 2500 kcal mol$^{-1}$ Å$^{-2}$, which is of the order of ten times the value expected for this term. In each minimisation, the M–S bond is forced to the exact input value, by virtue of the large M–S force constant used; the macrocycle must adjust conformation to meet with the requirements of the enforced M–S bond length. The minimised steric energy is an indication of the strain induced in the macrocycle by meeting the input M–S bond length. By plotting the calculated energy *versus* M–S bond length it is possible to deduce which bond length causes least strain in the ligands. To obtain more data around the minimum of each curve, further minimisations were performed at 0.05 Å intervals.

## Results and Discussion

*Synthesis.*—The two biphenyl polythiamacrocycle derivatives BIFS2O **6** and BIFS3 **7** were synthesised for the first time by reaction of 2,2′-bis(bromomethyl)-1,1′-biphenyl with bis(2-mercaptoethyl) ether (BIFS2O) or bis(2-mercaptoethyl) sulfide (BIFS3) under high dilution conditions. Scheme 1 describes these reactions. Yields were low and of the order of 10%, suggesting that the BIFS3 and BIFS2O macrocycle formation competes unfavourably with the formation of monothioether BIFS. Several attempts to improve these yields have been unsuccessful. Formation of the monothioether BIFS was unexpected, although there is a precedent in the literature.[27] Ochrymowycz and others suggested intrachain cyclisation (causing sulfonium ion formation) could result in the elimination of a *p*-dithiane fragment and a shortened chain in the macrocycle. This reaction was said to be favoured by the route used here. The yields of the BIFS in this work were greater in the case where *p*-thioxane would be eliminated, and in each case were much greater than those found in the reactions described by Ochrymowycz. The molecules BIFS3 and BIFS2O have been implemented as sensors in ISEs with identical composition to that used for **5**, 9S3,[16] for $Cu^{2+}$ detection; however, the BIFS3 and BIFS2O performances in ISEs were very poor in comparison to that of 9S3. However, implementation in ISEs for silver was more successful, with selectivities similar to those described previously for **2** and related compounds, and with generally similar performance.

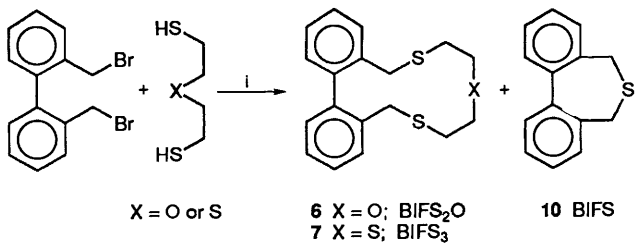


**Scheme 1** *Reagents:* i, 2 KOH, butan-1-ol

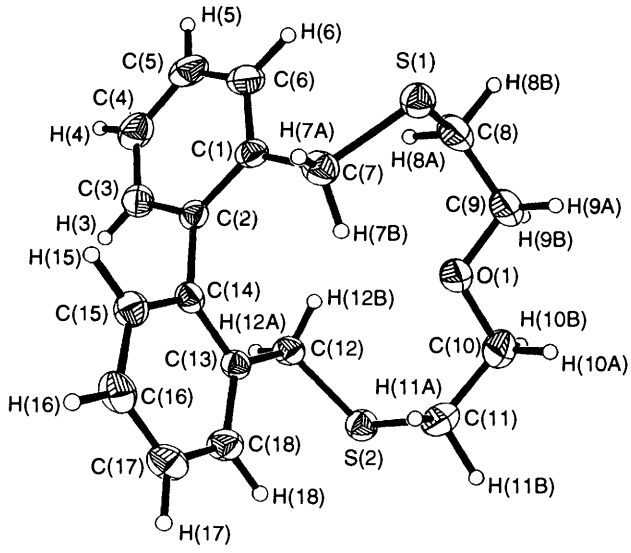


**Fig. 1** ORTEP plot and labelling scheme for the structure of **6**. Thermal ellipsoids are shown at 30% probability levels, except for the H atoms which are given with isotropic temperature factor $U$ = 1.0 Å$^2$.

*Crystal Structures.*—The crystal structure of BIFS2O **6** is shown in Fig. 1 and that of BIFS3 **7** in Fig. 2. Atomic coordinates, complete tables of bond distances and angles are collected in the Supplementary Data.* Selected geometric features of interest in the structure (shown in Table 2) include the torsion angles of the thioether segments of the macrocyclic ring and the ring torsion of the biphenyl unit. The definitions

* See footnote on p. 1310.

**Table 2** Selected details of geometries for **6–9** from molecular mechanics, and corresponding crystal structures of **6** and **7**

| | **6** crystal | **6** MM | **7** crystal | **7** MM | **8** MM | **9** MM |
|---|---|---|---|---|---|---|
| Tor1 | 70.16 | 72.9 | −177.3 | −177.5 | 72.1 | 180.0 |
| Tor2 | 66.98 | 72.9 | −178.6 | −177.2 | 72.4 | 179.7 |
| Tor3 | −92.75 | −94.0 | 112.0(2) | −119.1 | −93.1 | 101.9 |
| C(2)–C(14) | 1.5029 | 1.50 | 1.501(3) | 1.51 | 1.51 | 1.51 |

**Table 3** Definition of torsion angles used to describe simulations

| | **7**/**9** | **6**/**8** |
|---|---|---|
| Tor1 | S(1)–C(8)–C(9)–S(2) | S(1)–C(8)–C(9)–O(1) |
| Tor2 | S(2)–C(10)–C(11)–S(3) | O(1)–C(10)–C(11)–S(2) |
| Tor3 | C(1)–C(2)–C(14)–C(13) | C(1)–C(2)–C(14)–C(13) |

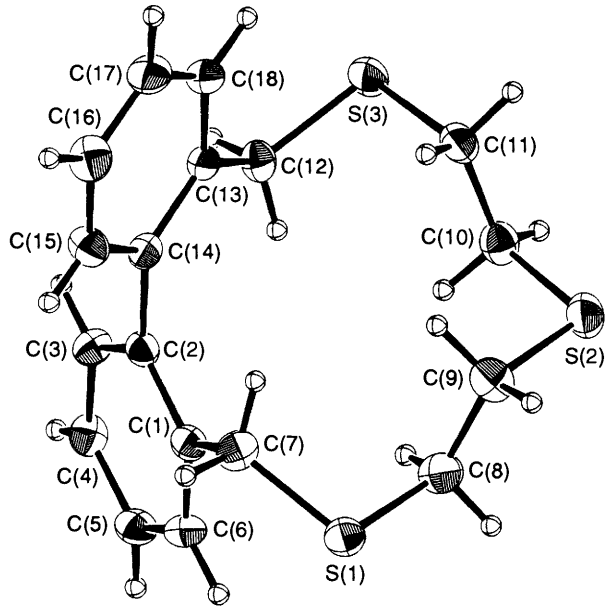


**Fig. 2** ORTEP plot and labelling scheme for the structure of **7**. Thermal ellipsoids are shown at 30% probability levels, except for H atoms which are drawn with isotropic temperature factor $U = 1.0$ Å$^2$.

of the torsion angles are given in Table 3. The BIFS3 structure has the biphenyl torsion of the macrocycle ring at 112.0°, which accommodates the typical bracket structure[10] of the thioether strand (two *anti* SCCS torsions) which would have to rearrange before this ligand could form chelate structures. The BIFS2O in contrast has the biphenyl torsion at −92.75° accommodating the two $g^+$ SCCO torsions. In this structure, the three donor atoms involved [S(1),O(1),S(2)] could not simultaneously form metal chelates without readjustment. In both **6** and **7**, the torsion of the biphenyl seems to be adjusting to the preferred geometry of the polythia (thioxa) strand, which provides an additional constraint.

*Molecular Dynamics.*—The biphenyl unit introduces certain stereochemical features which appear to be new to thiamacrocycle chemistry, and are of importance to the flexibility of the ligand. The torsion between two phenyl rings of the unit has a limited range of values. The unit itself is chiral, in the sense that it has right-handed and left-handed forms, based on the sign of the torsion between the two phenyl rings of the unit. The timescale for the reversal of the sign of the torsion is still expected to be much slower than the ps to ns timescale used in MD simulations, where torsional movement within a limited range, not leading to sign reversal, may be expected. The activation energy for racemisation would be increased by the addition to the unsubstituted *ortho* positions of substituents other than hydrogen. Compounds **8** and **9** were built and modelled to examine the effect of such additional substitution on the dynamics of the molecule on the ns timescale, as opposed to the timescale for racemisation.

**Table 4** Percentage populations of particular conformers from simulations

| Ligand | *T*/K | *gg* Same sign | *gg* Opposite sign | *ga* | *aa* |
|---|---|---|---|---|---|
| **6** | 300 | 8 | — | 92 | — |
| **6** | 350 | 16 | — | 84 | — |
| **6** | 470 | 24 | 21 | 21 | 34 |
| **7** | 300 | — | — | — | 100 |
| **7** | 350 | — | — | 20 | 80 |
| **7** | 470 | 5 | 1 | 51 | 43 |
| **8** | 300 | 44 | 29 | 27 | — |
| **8** | 350 | 52 | 26 | 22 | — |
| **8** | 470 | 44 | 27 | 29 | — |
| **9** | 300 | — | — | 24 | 76 |
| **9** | 350 | — | — | — | 100 |
| **9** | 470 | 11 | 11 | 63 | 15 |

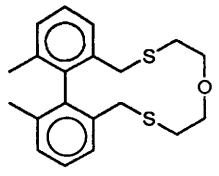


**8**

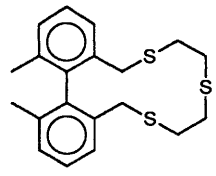


**9**

Following our earlier work on possible conformational rearrangements suggested by molecular dynamics (MD) simulations,[14,26] we carried out MD simulations of the new ligands, **6**, **7**, **8** and **9**. The results are presented in Tables 4–9 and Figs. 3–6. The features studied include the frequency of occurrence of the conformations traversed during the simulations (Table 4), the torsional movements (Figs. 3–6) and the comparison of the lowest energy conformations observed in the simulations (Tables 5–8). The movement of the macrocycle may be visualised in part from the trace of evolution of the relevant torsion angle (defined as in Table 3) with time (display method used in refs. 14 and 25). This type of display for sequences of individual conformers saved from each simulation enables recognition of genuine changes of conformation from inspection of plots.

In the crystal structure of **6**, the two SCCO segments have $g^+$ torsion angles. During simulation at 300 K, the two SCCO torsions tor1 and tor2 (see Table 3 for definition) switch mostly between *gauche* and *anti* torsion angles, while for comparison, there is no switching in the simulation of **7** at this temperature; switching for **6** becomes more frequent in higher temperature simulations. Fig. 3 shows the evolution of tor1 and tor2 at 300 K. The most surprising feature of this set of simulations was that very little time was spent in the $g^+,g^+$ conformation which was that found in the crystal structure. This is another instance in which the particular restraints of crystal packing

**Table 5** Energies of conformers of **6** from MD simulations

| Conformation | $T^a$/K | CHARMm energy/ kcal mol$^{-1}$ | Tor1 | Tor2 | Tor3 | Torsion combination |
|---|---|---|---|---|---|---|
| **6A** | 470 | 21.04 | 176.47 | 176.87 | −119.96 | *aa* |
| **6B** | 300 | 21.72 | 65.58 | 177.80 | −110.93 | $g^+a$ |
| **6C** | 300 | 24.13 | 72.38 | 71.64 | −92.50 | $g^+g^+$ |
| **6D** | 470 | 26.34 | 59.23 | −88.14 | −115.31 | $g^+g^-$ |

[a] Lowest temperature at which this conformation was found.

**Table 6** Energies of conformers of **7** from MD simulations

| Conformation | $T^a$/K | CHARMm energy/ kcal mol$^{-1}$ | Tor1 | Tor2 | Tor3 | Torsion combination |
|---|---|---|---|---|---|---|
| **7A** | 300 | 18.30 | 177.18 | 177.59 | 119.05 | *aa* |
| **7B** | 350 | 20.66 | 164.20 | −59.02 | 102.07 | $g^-a$ |
| **7C** | 470 | 23.47 | −72.20 | −72.29 | 82.61 | $g^-g^-$ |
| **7D** | 470 | 24.73 | 90.26 | −63.76 | 117.59 | $g^+g^-$ |

[a] Lowest temperature at which this conformation was observed.

**Table 7** Energies of conformers of **8** from MD simulations

| Conformation | $T^a$/K | CHARMm energy/ kcal mol$^{-1}$ | Tor1 | Tor2 | Tor3 | Torsion combination |
|---|---|---|---|---|---|---|
| **8A** | 300 | 19.62 | 174.36 | 62.89 | −99.31 | $g^+a$ |
| **8B** | 470 | 21.45 | 165.16 | −173.36 | −105.06 | *aa* |
| **8C** | 300 | 21.46 | 72.17 | 72.31 | −93.02 | $g^+g^+$ |
| **8D** | 470 | 24.06 | 101.36 | −56.77 | −99.69 | $g^-g^+$ |

[a] Lowest temperature at which this conformation was observed.

**Table 8** Energies of conformers of **9** from MD simulations

| Conformation | $T^a$/K | CHARMm energy/ kcal mol$^{-1}$ | Tor1 | Tor2 | Tor3 | Torsion combination |
|---|---|---|---|---|---|---|
| **9A** | 300 | 17.17 | 179.97 | 179.81 | 101.87 | *aa* |
| **9B** | 300 | 17.74 | 165.33 | −59.86 | 101.93 | $g^-a$ |
| **9C** | 470 | 22.76 | −63.74 | 80.10 | 91.86 | $g^-g^+$ |
| **9D** | 470 | 22.90 | 88.61 | 83.98 | 105.75 | $g^+g^+$ |

[a] Lowest temperature at which this conformation was observed.

**Table 9** Endodentate conformers isolated in MD simulations and generated conformations

| Conformation | $T^a$/K | CHARMm energy/ kcal mol$^{-1}$ | Tor1 | Tor2 | Tor3 | Torsion combination |
|---|---|---|---|---|---|---|
| **6E** | 470 | 27.38 | 43.94 | −61.74 | −104.18 | $g^+g^-$ |
| **9E** | 470 | 22.96 | 55.03 | −75.66 | 90.69 | $g^+g^-$ |
| **7E** | *b* | 26.67 | 44.72 | −63.82 | −108.80 | $g^+g^-$ |
| **8E** | *c* | 26.13 | 55.25 | −71.67 | 87.96 | $g^+g^-$ |
| **6F** | 470 | 29.6559 | −42.99 | −67.75 | −111.10 | $g^-g^-$ |

[a] Lowest temperature at which this conformation was observed. [b] Generated from **6E** by substituting S for O and minimising. [c] Generated from **9E** by substituting O for S and minimising.

have created one structure, while simulation of gas-phase behaviour suggests another structure.

Results for simulation of **7** at 300, 350 and 470 K are presented next. The coordination vectors for sulfur in the crystal conformation are suitable for exodentate binding to metal ions. Other conformers were reached during the simulations in which either one of the SCCS torsions became *gauche*. Structures with both SCCS torsions *gauche* were transitory. The simulation of **7** at 300 K reveals little change from the starting conformation; at 350 K, tor2 (see Table 3) moves through $g^+$, *a* and $g^-$ configurations, with little change in tor1; at the same time, tor3, the biphenyl torsion, exhibits small changes reflecting the change in tor2, but always within the range of 120 to 80°. That the tor3 angle is changing rapidly on the ps–ns timescale, is consistent with the findings that torsion angles measured by some physical techniques represent a time-average.[6] The simulation at 470 K indicates greater mobility, with tor1 spending several periods in a $g^-$ conformation: tor2 is *anti* during much of this period of the evolution. However, long periods in which both segments have *anti* torsions as in the crystal structure are still evident (see Fig. 4).

The addition of methyl groups to the sterically important

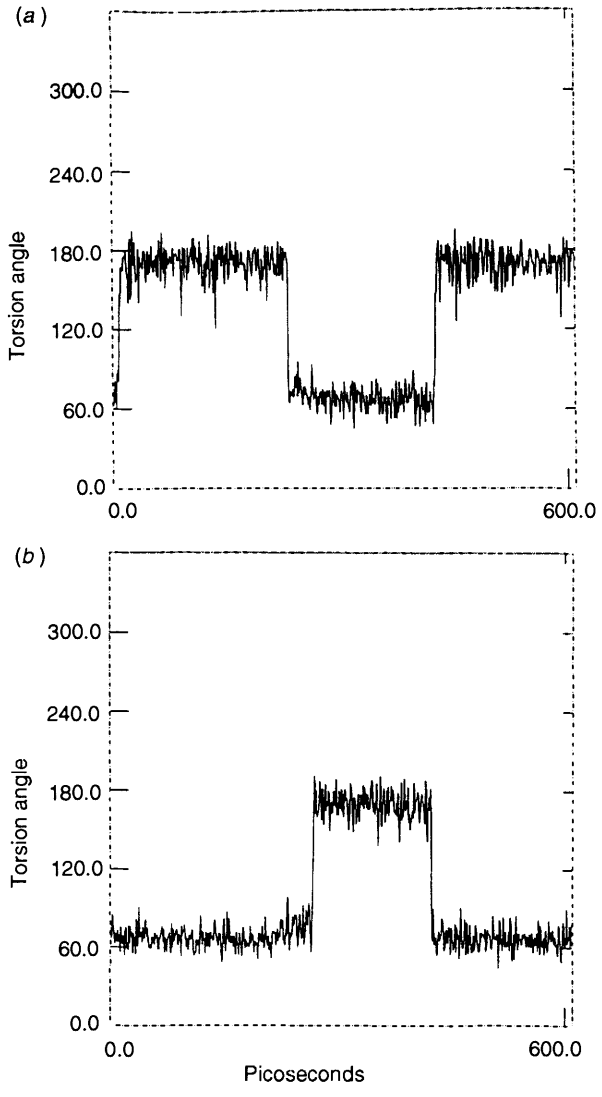


**Fig. 3** Variation of tor1 (*a*) and tor2 (*b*) in MD simulation of **6** at 300 K

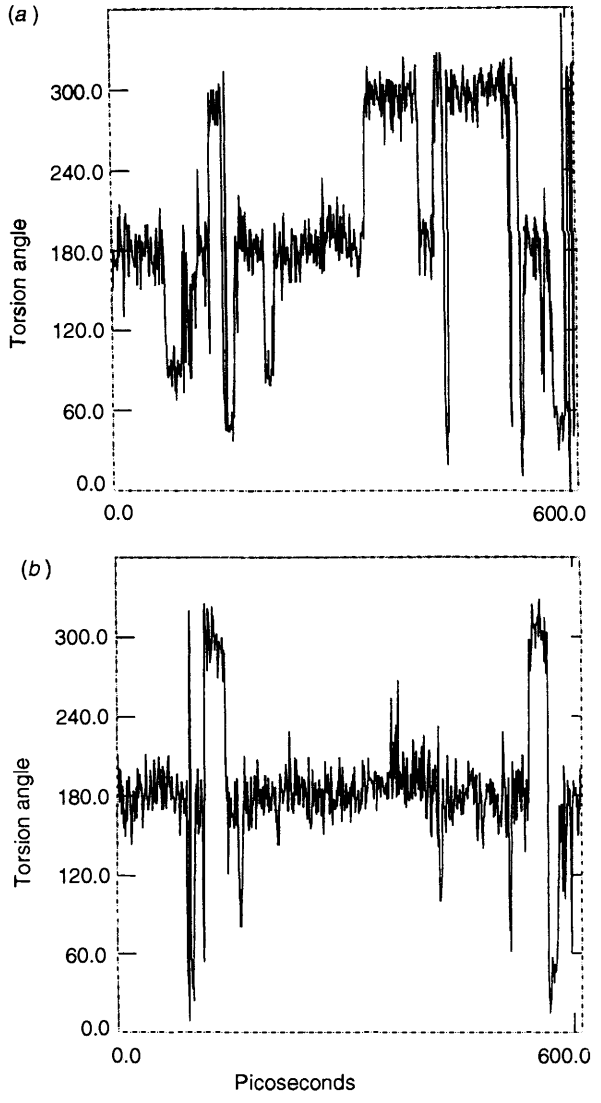


**Fig. 4** Variation of tor1 (*a*) and tor2 (*b*) in MD simulation of **7** at 470 K

remaining *ortho* positions imposes a steric barrier to twisting of the biphenyl torsion, perhaps restricting the mobility of the system, and has been realised in practice by Rebek and co-workers for some crown ethers.[9] In another attempt to limit accessible conformations in the simulations described here, **8** was generated by the addition of methyl groups to the remaining *ortho* positions of the biphenyl unit in **6**. Again tor1 and tor2 switch between *a* and $g^+$ configurations, although significant time is spent with both angles $g^+$, which is not the case in the simulation of **6**. One simulation is shown in Fig. 5.

The molecule **9** (built from **7** with the Molecular Editor of CHARMm for our calculations) was apparently more mobile than **7**, as seen in MD simulations at 300 K (see Fig. 6); this was against our initial expectation, perhaps because the added restriction to tor3 prevented movement there, so that the thermal energy distributed more into the bracket torsions, tor1 and tor2.

The lowest energy conformers found for each ligand **6**, **7**, **8** and **9** are shown in Tables 4–7, further characterised by the values of the three torsions tor1, tor2 and tor3 (previously defined in Table 3). The lowest energy conformers obtained are assumed to be the ground state in subsequent discussion. It can be seen that *a,a* conformers appear to be the more stable for both **6** and **7**, and that an *a,g* conformer lies closer in energy to these for **6** than for **7**. The lowest energy $g^+,g^+$ conformer found for **6** (which is the conformation also seen in the crystal structure) was 3.082 kcal $mol^{-1}$ higher in energy than that calculated for the lowest observed *a,a* conformation. The lowest energy conformer found in the simulation of **8** had tor1 and tor2 values which were *g,a* as the ground state, with the lowest energy *a,a* conformer 1.834 kcal $mol^{-1}$ higher. The lowest energy conformer found in simulation of structure **9** was *a,a* as for **7**, with *a,g* conformers within 0.6 kcal $mol^{-1}$. The postulated methyl substitution apparently reduces the twist range available for the ar-C–ar-C torsion, and stabilises different conformers, the *a,a* conformers being destabilised for both **8** and **9**. The substitution in **8** apparently stabilises a different ground state from that of **6**, while the same ground state conformation is observed for **7** and **9**. For both **6** and **7**, addition of methyl groups (**8**, **9**) increases the proportion of *g,a* conformers accessed in the simulations.

Endodentate conformations were only found in the simulations at 470 K of **9**, and BIFS2O, **6**; details are shown in Table 9. By changing the relevant central heteroatom of the bracket (S to O or *vice versa*) using the Molecular Editor of QUANTA, endodentate conformations of BIFS3, **7**, and of **8**, were built (from **6E** and **9E** respectively). Details of the minimised structures are shown in Table 9. It became apparent that not all $g^+,g^-$ torsion combinations resulted in endodentate conformations. However, a unique conformer **6F** with $g^-,g^-$ torsion combination adopted an endodentate conformation. This is included in the table of endodentate conformers found.

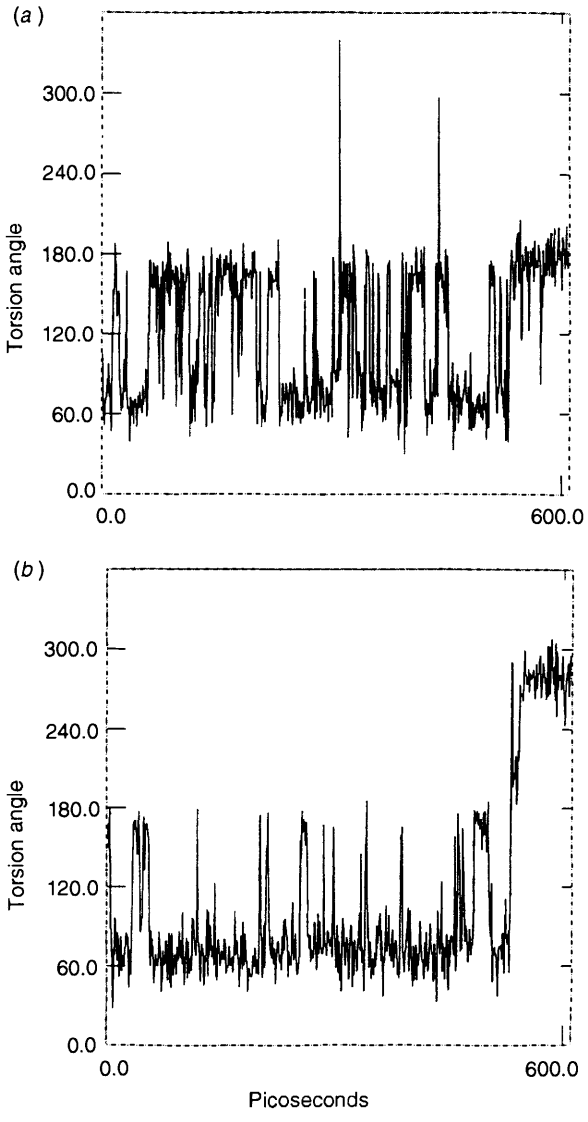


**Fig. 5** Variation of tor1 (*a*) and tor2 (*b*) in MD simulation of **8** at 470 K

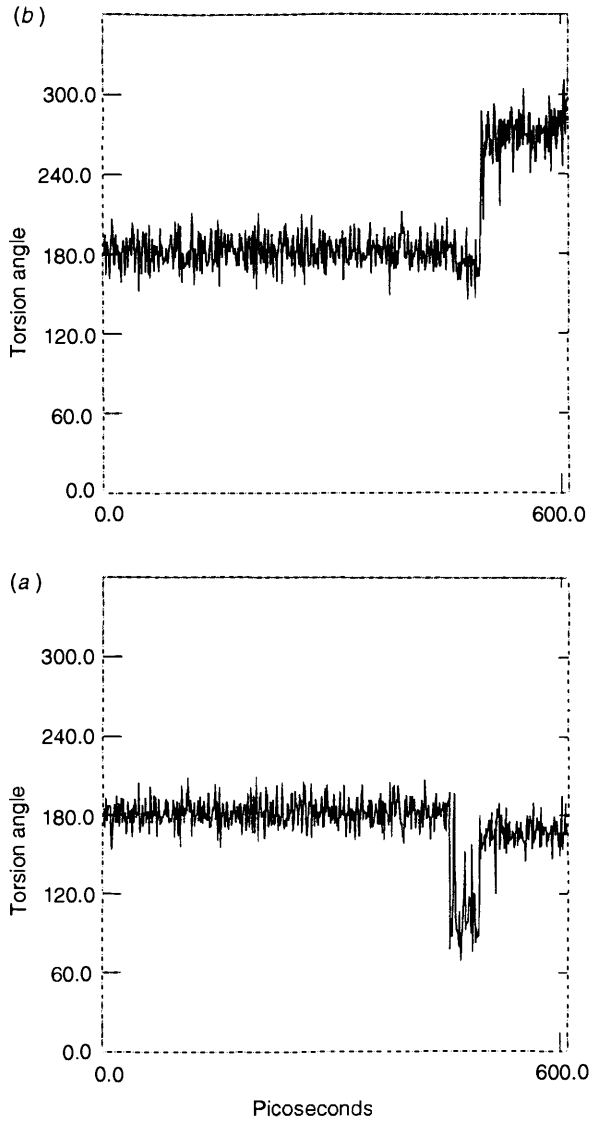


**Fig. 6** Variation of tor1 (*a*) and tor2 (*b*) in MD simulation of **9** at 300 K

In all of these instances *endo* conformers, with *gauche* values for tor1 and tor2 were between 4 and 7 kcal $mol^{-1}$ higher in energy than the relevant ground state. These are the conformers of interest for the formation of two chelate rings simultaneously by the ligand. Biphenyl torsions for the Rebek crown ethers[9] with a similar dimethylbiphenyl unit were calculated from the crystal data for CEDNAA (compound **11**),[9] obtained from the Cambridge Crystallographic Database[28] as 70.7° and for CEDNEE (compound **12**),[9] as −88.6°. In these structures, a mercury(II) ion is chelated by the ether oxygens, forcing the biphenyl torsion to adopt a low value. These values should be compared with those in Table 9.

For comparison with other work,[14] the lowest energy *endo* geometries found for **7** and **9** were analysed to determine the optimum ring size likely to be displayed on coordination to a metal ion. One striking feature of these theoretical calculations is the implication that the effect of adding methyl groups causes **9** to have a much smaller optimal hole size than **7**. The respective hole sizes of **7**, the BIFS3 and **9**, the *ortho*-methylated BIFS3 species, acting as tridentate ligands, were calculated using the method developed by Drew, Hollis and Yates,[17] and the plots are shown in Figs. 7 and 8. It is immediately noticeable that the optimal M–S bond length of **9** is significantly shorter, by 0.15 Å than that for **7**. The optimal M–S bond length of

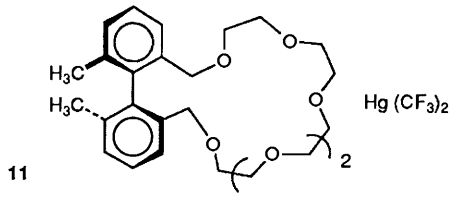


**11**

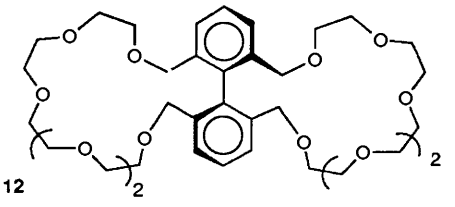


**12**

BIFS3 we calculate to be 2.70 Å, and of *o*-Me-BIFS3 to be 2.55 Å. We have noted a similar result with 9S3, **5**, and a 2,5,8-trimethyl-substituted 9S3 ligand.[18] Thus, it seems that introducing 'locking groups' to macrocycles could be a way of designing new ligands with specific geometric requirements, which may be of use in the design of specific metal-selective ligands.

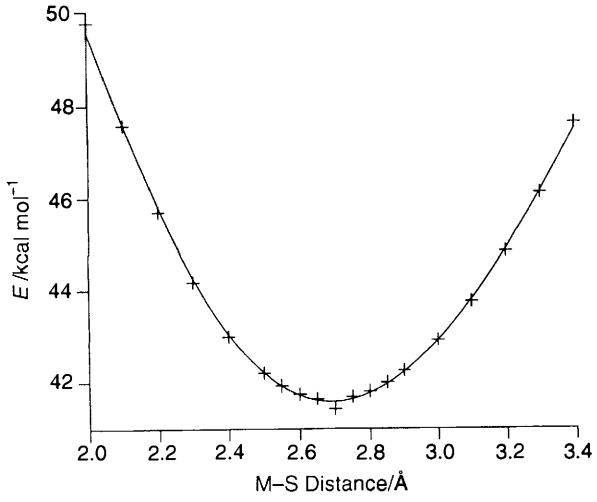


**Fig. 7** Plot of steric energy (MM) *versus* M–N distance for **7**

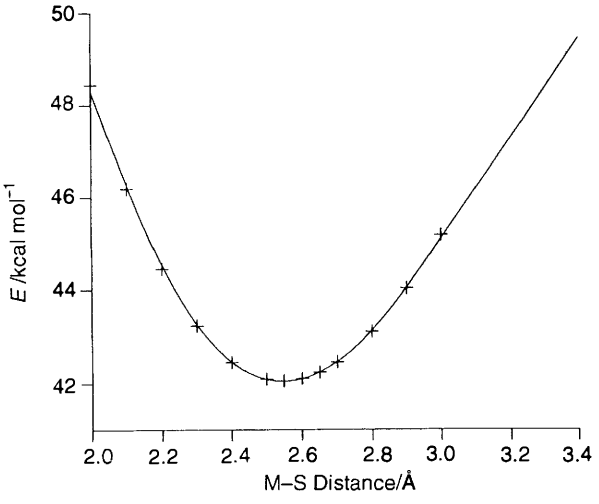


**Fig. 8** Plot of steric energy (MM) *versus* M–N distance for **9**

## Conclusions

The presence of the biphenyl aromatic hinge has several effects by comparison with the cyclophanes **2–4** studied previously.[14] The end sulfurs can approach each other more freely. Torsion around the ar-C–ar-C link is possible (within a limited range of *ca.* 30°) which makes the molecules much more mobile than, say, the corresponding *p*-cyclophane, **4**. The effect of this mobility on their ability to coordinate different metal ions will be an important study. Calculations of the effect of blocking the remaining *ortho* positions with methyl groups indicated an effect on the switching rate of the simulated dimethyl molecules **8** and **9** but considerable changes in the proportions of different conformers traversed. The biggest change calculated was the decrease in hole size observed for the BIFS3 molecule on methylation. This change in design has suggested an important feature for future syntheses of trithiamacrocycles.

## Acknowledgements

The authors are grateful for support from SERC and the Brite-Euram Program, CICYT (Spanish Government) MAT91-0952, and thank Dr M. G. B. Drew for divulging the results in ref. 19 prior to publication.

## References

1 J. Trotter, *Acta Crystallogr.*, 1961, **14**, 1135.
2 O. Bastiansen, *Acta Chem. Scand.*, 1949, **3**, 408.
3 A. Almenningen, O. Bastiansen, L. Fernholt, B. N. Cyvin, S. J. Cyvin and S. Samdal, *J. Mol. Struct.*, 1985, **128**, 59.
4 G. Celebre, G. Deluca, M. Longen, D. Catalano, C. A. Veracini and J. W. Emsley, *J. Chem. Soc., Faraday Trans.*, 1991, **87**, 2623.
5 S. Tsuzuki and K. Tanabe, *J. Phys. Chem.*, 1991, **95**, 139.
6 J. L. Baudour, *Acta Crystallogr., Sect. B*, 1991, **47**, 935.
7 L. D. Field, B. W. Skelton, S. Sternhell and A. H. White, *Aust. J. Chem.*, 1985, **38**, 391.
8 E. P. Kyba, M. G. Siegel, L. R. Sousa, G. D. Y. Sogah and D. J. Cram, *J. Am. Chem. Soc.*, 1973, **95**, 2691.
9 J. Rebek, T. Costello, L. Marshall, R. Wattley, R. C. Gadwood and K. Onan, *J. Am. Chem. Soc.*, 1985, **107**, 7481.
10 S. R. Cooper and S. C. Rawle, *Struct. Bonding*, 1990, **72**, 1.
11 A. J. Blake and M. Schroeder, *Adv. Inorg. Chem.*, 1990, **35**, 1.
12 J. Casabó, C. Pérez-Jiménez, L. Escriche, S. Alegret, E. Martínez-Fábregas and F. Teixidor, *Chem. Lett.*, 1990, 1107; J. Casabó, L. Mestres, L. Escriche, F. Teixidor and C. Pérez-Jiménez, *J. Chem. Soc., Dalton Trans.*, 1991, 1969; Z. Brzozka, P. L. M. H. Cobben, D. N. Reinhoudt, J. J. H. Edema, J. Buter and R. M. Kellog, *Anal. Chim. Acta*, 1993, **273**, 139.
13 M. Muroi, T. Kamiki and E. Sekido, *Bull. Chem. Soc. Jpn.*, 1989, **62**, 1797.
14 J. C. Lockhart, D. P. Mousley, M. N. Stuart Hill, N. P. Tomkinson, F. Teixidor, M. P. Almajano, L. Escriche, J. Casabó, R. Sillanpää and R. Kivekäs, *J. Chem. Soc., Dalton Trans.*, 1992, 2889.
15 B. de Groot and S. J. Loeb, *Inorg. Chem.*, 1990, **29**, 4084; *J. Chem. Soc., Chem. Commun.*, 1990, 1755; B. de Groot, G. S. Hanan and S. J. Loeb, *J. Am. Chem. Soc.*, 1991, **30**, 4645; B. de Groot, G. R. Giesbrecht, S. J. Loeb and G. K. Shimizu, *Inorg. Chem.*, 1991, **30**, 177.
16 M. A. Flores, F. Teixidor, L. Escriche and J. Casabó, unpublished work.
17 M. G. B. Drew, S. Hollis and P. C. Yates, *J. Chem. Soc., Dalton Trans.*, 1985, 1829.
18 G. A. Forsyth and J. C. Lockhart, unpublished work.
19 J. Beech, P. J. Cragg and M. G. B. Drew, *J. Chem. Soc., Dalton Trans.*, 1994, 719.
20 G. M. Sheldrick, SHELXS86, *Program for the Solution of Crystal Structures*, Univ. of Gottingen, Germany, 1986.
21 *XTAL 3.0 Reference Manual*, ed. S. R. Hall and J. M. Stewart, Univ. of Western Australia and Maryland, 1990.
22 C. J. Gilmore, *J. Appl. Crystallogr.*, 1982, **17**, 42.
23 TEXSAN-Texray, *Single Crystal Structure Analysis Package, Version 5.0*, Molecular Structure Corporation, The Woodlands, TX, 1989.
24 C. K. Johnson, *ORTEP-II, Report ORNL-5138*, Oak Ridge National Laboratory, Oak Ridge, TN, 1976.
25 J. C. Lockhart and N. P. Tomkinson, *J. Chem. Soc., Perkin Trans. 2*, 1992, 533.
26 CHARMm version 21. B. R. Brooks, R. E. Bruccoleri, B. D. Olafson, D. J. States, S. Swaminathan and M. Karplus, *J. Comp. Chem.*, 1983, **4**, 187.
27 L. A. Ochrymowycz, C. P. Mak and J. D. Michna, *J. Org. Chem.*, 1974, **39**, 2079.
28 F. H. Allen, J. E. Davies, J. J. Galloy, O. Johnson, O. Kennard, C. F. Macrae, E. M. Mitchell, G. F. Mitchell, J. M. Smith and D. G. Watson, *J. Chem. Inf. Comp. Sci.*, 1991, **31**, 187.

*Paper* 3/07267C
*Received* 8*th December* 1993
*Accepted* 28*th January* 1994